Scientific Reports

https://doi.org/10.1038/s41598-026-41839-y

Article in Press

Analysis of the resistance of small peptides from *Periplaneta americana* to H_2O_2-induced apoptosis in KGN Cells based on miRNA-seq

Received: 30 August 2025

Accepted: 23 February 2026

Published online: 01 March 2026

Cite this article as: Xu L., Jiang R., Su J. *et al.* Analysis of the resistance of small peptides from *Periplaneta americana* to H_2O_2-induced apoptosis in KGN Cells based on miRNA-seq. *Sci Rep* (2026). https://doi.org/10.1038/s41598-026-41839-y

Linjie Xu, Rong Jiang, Jingjing Su, Ruixian Sun, Lilian Yang, Yunping Tang & Shiyan Sui

Analysis of the Resistance of Small Peptides from *Periplaneta americana* to H_2O_2-induced Apoptosis in KGN Cells based on miRNA-seq

Linjie Xu[1†], Rong Jiang[1†], Jingjing Su[2], Ruixian Sun[1], Lilian Yang[1], Yunping Tang[1], Shiyan Sui[1,3*]

1 College of Public Health, Dali University, Dali, 671000, China

2 Management Department of Laboratory, Dali University, Dali 671000, China

3 Yunnan Provincial Key Laboratory of Entomological Biopharmaceutical R&D, Dali, 671000, China

*Corresponding authors: College of Public Health, Dali University, Dali City, Yunnan, 671000, China. E-mail: lapletian689@163.com

†Linjie Xu and Rong Jiang shared co-first authorship

Abstract

Apoptosis of ovarian granular cells is closely related with weakening fertility of women. Hence, resisting apoptosis of human ovarian granular cells (KGN cells) is of important significance. According to studies, detection of oxidation indicators such as ROS, NO, MDA and SOD, DAPI fluorescence staining experiment, mRNA and Western Blot test of Cleaved-caspase-3, Caspase-3, Bax and Bcl-2 demonstrate that small peptides from Periplaneta americana (SPPA) can improve H_2O_2 -induced apoptosis of KGN cells. While SPPA has been reported to possess antioxidant potential, its specific role and molecular mechanisms within ovarian granulosa cells particularly regarding its involvement in the miRNA regulatory network have not yet been thoroughly investigated.

Therefore, high-throughput sequencing of miRNAs was employed to identify differentially expressed miRNAs (DEMs) that are associated with the regulatory mechanisms through which SPPA inhibits H_2O_2-induced apoptosis in KGN cells. Experiments were divided into three groups, namely, the control group, H_2O_2 group and H_2O_2 + SPPA group. A total of 75 DEMs were screened by comparing the control group and the H_2O_2 group, and 30 DEMs were screened by comparing the H_2O_2 group and H_2O_2 + SPPA group. It is important to note that 8 overlapping DEMs were identified upregulating in H_2O_2 exposure, but downregulating in SPPA repair. Another 5 overlapping DEMs were identified downregulating in H_2O_2 exposure, but upregulating in SPPA repair. 3534 target genes of the aforementioned 13 DEMs have significant enrichment in multiple KEGG pathways. Among them, hsa-miR-103a-3p, NovelmiRNA-214 and NovelmiRNA-383 play significant roles in SPPA resistance process of cell apoptosis. 5 DEMs were selected for florescence quantitative PCR (qPCR) verification and the expression level was consistent with sequencing results. Finally, a control network of SPPA resistance against the H_2O_2-induced KGN cell apoptosis was built based on the target genes screened by the miRNA-seq technology. This study provides a direction and some references to screen and suggest miRNAs that may be involved in the anti-apoptotic process of SPPA.

Keywords: Small peptides from *Periplaneta americana,* Oxidative stress, Apoptosis, MicroRNA, High-throughput sequencing

1 Introduction

Premature ovarian failure (POF) is a prevalent gynecological endocrine disorder characterized by the loss of

ovarian function due to factors such as follicle depletion, follicle atresia, or chemotherapy, occurring before the age of 40. Research indicates that the global incidence of POF has reached 3.7%[1] and is gradually becoming more common among younger populations. Follicle atresia is a normal physiological phenomenon that occurs during follicle development, however, abnormal follicle atresia can lead to a reduction in the number of available follicles, a decrease in the number of ovulations, and ultimately, a decline in fertility[2]. The underlying mechanism of follicle atresia involves the apoptosis of follicle granulosa cells(GCs)[3].

Oxidative stress refers to the pathological biochemical reaction that occurs when the balance between reactive oxygen species (ROS) generated in the body and the antioxidant system is disrupted[4]. Studies have confirmed that oxidative stress can induce apoptosis in human ovarian granule cells (KGN cells), which may lead to POF[5]. *Periplaneta americana* (PA), which originates from South America, belongs to the family Blattaria. Despite being a global pest that damages clothing, contaminates food, and spreads diseases, humanity benefits from the pharmacological properties of compounds derived from this species. It exerts anti-inflammatory[6] and wound repair[7] functions. Small peptides from *Periplaneta americana* (SPPA) is a peptide-based extract obtained from the desiccated body of *Periplaneta americana*, with small peptides constituting 94.44% of this extract[8]. Our research team has discovered that SPPA exhibits anti-oxidative and anti-apoptotic effects. For example, fu demonstrated that SPPA inhibits H_2O_2-induced apoptosis in KGN cells by mediating mitochondrial autophagy through

Bcl2L13[9]. Furthermore, SPPA also inhibits H_2O_2-induced human KGN cells apoptosis through antioxidation, and the SIRT1/p53 signal pathway mediates the antioxidation[10]. MiRNAs, as key regulators of gene expression, may play a significant role in this intricate mechanism.

MicroRNAs (miRNAs) are a class of endogenous non-coding RNAs (ncRNAs) with regulatory functions in eukaryotes, typically ranging from 18 to 24 nucleotides(nt) in length by binding to the 3′-UTR region of mRNAs, miRNAs mediate mRNA degradation or inhibit translation, thereby regulating gene expression post-transcriptionally[11]. It has been shown that miRNAs are involved in the regulation of reproduction in animals, including oocyte differentiation, growth, development and the synthesis of ovulation-related hormones[12]. Currently, studies have reported that cells undergoing oxidative stress, such as those involving miR-192 targeted Acvr2a to promote caspase-3 apoptotic signaling pathway[13], miR-30a-5p inhibits granulosa cell death by inhibiting Beclin1[14], and -miR-130b-3p affects the KEAP1/NRF2 pathway in GCs by modulating SESN2 expression in response to oxidative stress damage[15], regulate granulosa cell apoptosis by modulating target genes and their associated signaling pathways. However, the precise mechanism by which miRNAs are modulated by SPPA following oxidative stress-induced apoptosis in KGN cells remains unclear.

MiRNA sequencing is a high-throughput technology that systematically identifies and quantifies miRNAs. Currently, it has become a standard technique in the field of microRNA research, significantly advancing the discovery of disease biomarkers[16]. In

this study, we analyzed differentially expressed miRNAs that are regulated by SPPA in the context of H_2O_2-induced apoptosis in KGN cells. We also examined the target genes, enrichment pathways, and biological functions associated with these differentially expressed miRNAs. These findings preliminarily screen and suggest miRNAs that may be involved in the anti-apoptotic process of SPPA.

2 Materials and methods

2.1 Cell culture and establishment of apoptosis model

KGN cells were generously provided by Dr. Liu Jie from Nanjing Agricultural University (catalog number: H057). Professor Liu Guangming from Dali University provided the SPPA. The specific cell culture method has been described in our latest study[10]. The cells were categorized into three groups: the control group (K, n = 2 × 4), which consisted of KGN cells with an 85-90% cell fusion rate; the H_2O_2 group (H, n = 2 × 4), which included KGN cells in normal culture supplemented with 250 μmol/L H_2O_2 solution and treated continuously for 6 hours; and the H_2O_2+SPPA group (C, n = 2 × 4), which comprised cells from the H_2O_2 group that were additionally treated with 50 μg/mL SPPA solution and incubated for 12 hours. Here, "n = 2 × 4" indicates that each group consisted of eight wells for cell culture, with every four replicate wells collected in a centrifuge tube. Thus, K1 = $K_{1\sim4}$, K2 = $K_{5\sim8}$.

2.2 Cell counting kit-8 (CCK-8) assay

KGN cells were digested with 0.25% trypsin (WISENT), seeded into 96-well plates at a rate of 1 × 10^4 cells/well and allowed to culture for 24 hours. After the different treatments, the cell viability was measured using a CCK-8 (Meilunbio). The original medium was discarded, and 100 μL of the culture medium (15% fetal bovine serum or serum-free) containing 10% CCK-8 solution

was added to each well. After incubation for 1.5 hours, the OD value was recorded at 450 nm using a microplate reader.

2.3 Evaluation of SPPA resistance to apoptosis in KGN cells

2.3.1 Detection of reactive oxygen species (ROS), malondialdehyde (MDA), superoxide dismutase (SOD), and nitric oxide (NO)

The cells were treated with 250 μmol/L H_2O_2 for 6 hours, followed by the addition of 50 μg/mL SPPA solution for 12 hours. According to the kit instructions (Beyotime Biotechnology Co., Ltd., Shanghai, China), first, add the ROS-positive control stimulation. Next, introduce the fluorescent probes and incubate the mixture for 30 minutes. Finally, capture images using a fluorescence microscope. Upon completion of the photography, the cells were harvested and quantified. The fluorescence intensity of the cells was measured at an excitation wavelength of 488 nm and an emission wavelength of 525 nm using a fluorescence microplate reader. The MDA level in the cells was determined at 532 nm using a MDA assay kit (Beyotime Biotechnology Co., Ltd., Shanghai, China). The SOD content in the culture medium was measured at 450 nm using a SOD assay kit (Beyotime Biotechnology Co., Ltd., Shanghai, China), and the NO content in the culture medium was measured at 540 nm using a NO assay kit (Beyotime Biotechnology Co., Ltd., Shanghai, China).

2.3.2 Real-time quantitative PCR (qPCR) of genes

Total RNA was extracted from cells using RNA-easy lsolation Reagent. The total RNA was converted to cDNA using a Reverse Transcription System (TIANGEN). QPCR was performed with SYBR Green (TIANGEN). The reaction programme was as follows: predenaturation at 95℃ for 15min, then 95℃ for 10s and 60℃ for 32s for 40 amplification cycles. Expression data were normalized to

β-actin expression. The primer sequences of these genes are listed in Table 1.

2.3.3 Cell apoptosis was measured by DAPI (4′,6-diamidino-2-phenylindole) staining

Cells treated with or without H_2O_2 were stained with DAPI for 5 min at room temperature (Beyotime Biotechnology Co., Ltd., Shanghai, China), and then examined under a fluorescence microscope (Nikon Imaging Equipment Sales Co., Ltd., Beijing, China). Thirty random fields were studied in each replicate. Apoptosis was defined as nuclear condensation, and the results are expressed as the ratio of the number of apoptotic cells/the total number of nucleus, per field[17].

2.3.4 Western blot (WB)

The cells were treated with 250 μmol/L H_2O_2 for 6 hours, followed by the addition of 50 μg/mL SPPA solution for 12 hours. Cells were then collected, and the cell lysates were prepared using lysis buffer. An enhanced BCA protein assay kit (Beyotime) was used to detect the protein concentration. Aliquots of the cell lysates (50 μg per sample) were subjected to 10% sodium dodecyl sulphate-polyacrylamide gel electrophoresis and then electroblotted onto nitrocellulose membranes (Biotrace). After blocking with 5% skim milk powder (BioFroxx) at room temperature for 1.5 hours, the primary antibodies against Bcl-2, Bax (Beyotime), Cleaved-caspase-3, Caspase-3 and β-actin (Bioworld) were added and incubated at 4℃ overnight. Next, the secondary antibody (Bioworld) was incubated at room temperature for 1.5 hours. The protein band was observed using a chemiluminescent system.

2.4 RNA extraction, library preparation, and sequencing

RNA extraction, library construction and miRNAs sequencing were conducted by GENEWIZ. Total RNA of each sample was extracted using TRIzol Reagent/ miRNeasy Mini Kit(Qiagen). Total RNA of each sample was quantified and qualified by Agilent 2100/2200 Bioanalyzer (Agilent Technologies, Palo Alto, CA, USA), NanoDrop (Thermo Fisher Scientific inc.) and 1% agrose gel. The suitable volume of total RNA was used for following library preparation. Next generation sequencing library preparations were constructed according to the manufacturer's protoco. 3′ SR and 5′ SR adaptor for Illumina was ligated to the small RNA using 3′ and 5′ ligation enzyme and first strand cDNA was synthesized using ProtoScript II Reverse Transcriptase. Each sample was then amplified by PCR. The PCR products of ~150 bp were recovered and cleaned up using PAGE, validated using an Agilent 2100/2200 Bioanalyzer (Agilent Technologies Palo Alto, CA, USA), and quantified by Qubit 3.0 Fluorometer (invitrogen, Carlsbad, CA). In order to remove technical sequences, including adapters, PCR primers, or fragments thereof, and quality of bases lower than 20, pass filter data of fastq format were processed by Trimmomatic (v0.30) to be high quality clean data.

2.5 Small RNA sequencing data analysis and identification of candidate novel miRNAs

We employed FastQC to assess the sequencing quality, focusing on the average base quality distribution and GC content. Following this, adapter sequences and low-quality reads were removed using Trimmomatic. Subsequently, we conducted a statistical analysis of the length and quantity of the resulting sequences. The length distribution statistics serve as a verification of the experiment's reliability. To differentiate among non-coding RNA types such as miRNA, rRNA, and tRNA, we compared our

results with the Rfam database. Utilizing the characteristic hairpin structure of miRNA precursors, we employed miRDeep2 software to predict and score the secondary structure of unannotated genome-aligned sequences, thereby screening for candidate novel miRNAs.

2.6 Identification of differentially expressed miRNAs

Differential expression analysis used the DESeq/ DESeq2 Bioconductor package, a model based on the negative binomial distribution. After adjusted by Benjamini and Hochberg's approach for controlling the false discovery rate and were screened according to the criteria of Fold Change $\geq$ 2 and $P \leq 0.05$. This study employed venn diagrams and volcanic plots to illustrate DEMs and to quantify the upregulation and downregulation of differential expressions between different groups. Hierarchical clustering analysis was performed on the expression levels using the CPM values (CPM = miRNA reads counts $\times$ 10^6 / total reads) of different groups. This approach aggregated miRNAs with similar functions or close relationships into classes, enabling the identification of functions for unknown miRNAs and the exploration of unknown functions for known miRNAs, thereby inferring their potential joint involvement in the same biological process or cellular pathway.

2.7 Functional annotation of target genes for differentially expressed miRNAs.

The miranda software (v 3.3a) was employed to predict the miRNA target genes for the corresponding species. The prediction was based on specific evaluation criteria: a sequence alignment score exceeding 150 and an absolute value of the binding free energy (ΔG) greater than 30. To assess the functions, roles, and biological processes of the target genes for DEMs and their

enrichment in different biological pathways. What biological functions are significantly associated with these target genes as determined by Gene Ontology (GO) analysis. Furthermore, Kyoto Encyclopedia of Genes and Genomes (KEGG) analysis identified the primary biochemical metabolic pathways and signal transduction pathways associated with these target genes. The gene symbols were entered into the database for annotation, visualization and integrated discovery (DAVID) online tool (https://david.ncifcrf.gov/home.jsp) to retrieve functional items and KEGG signaling pathways related to these genes in GO enrichment analysis. Subsequently, the enrichment results and expression patterns of these DEMs were visualized using the online tool microbioinformatics (https://www.bioinformatics.com.cn/).

2.8 Constructing the miRNA-mRNA regulatory network

Based on the targeted regulatory relationship between miRNAs and mRNA, the miRNA-mRNA regulatory network was constructed and visualized using cytoscape software and the STRING online tool.

2.9 qPCR of DEMs

Total RNA was extracted from KGN cells using TRIzol Reagent (Life Technologies, China) and subsequently processed with a kit from Takara (Japan) to determine RNA concentration. After confirming the purity of the RNA samples, the miRNA first-chain cDNA synthesis kit (Sangon, China) was utilized for the reverse transcription of 2 μg of total RNA. Aliquots of cDNA (2 μL) were diluted 150-fold for qPCR. Differentially expressed miRNAs were analyzed using specific upstream primer sequences designed and synthesized by Sangon (Shanghai). The reaction programme was as follows: predenaturation at 95℃ for 30s, then 95℃ for 5s and 63℃ for 30s for 40 amplification cycles. The universal downstream

primer U6 served as an internal reference gene in the kit. Specific forward primer sequences for DEMs were designed and synthesized by Sangon (Table 2). The specificity of the primers was evaluated through integration curve analysis and sequencing of the PCR products.

2.10 Statistical analysis

All data are expressed as mean ± SEM, and one-way ANOVA was conducted using SPSS 21.0. The least significant difference (LSD) method was employed for pairwise comparisons. The relative expression levels of each gene were calculated using the $2^{-\Delta\Delta Ct}$ method. Histograms were generated using GraphPad Prism 10.4.2, with $P < 0.05$ indicating a statistically significant difference.

3 Results

3.1 Determination of the optimal concentration and duration of H_2O_2-induced apoptosis in KGN cells.

When the CCK-8 solution was prepared using a culture medium supplemented with 15% fetal bovine serum, the survival rates of KGN cells treated with 150, 200, and 250 μmol/L H_2O_2 for 2, 4, and 6 hours did not show a significant downward trend compared to the control group (0 μmol/L); instead, they increased (Fig. 1A-D). Conversely, when the CCK-8 solution was prepared using serum-free culture medium, the survival rates of KGN cells treated with the different concentrations of H_2O_2 for 2, 4, and 6 hours all decreased compared to the control group (Fig. 2). Specifically, the cell viabilities after 2 hours of H_2O_2 treatment in 150, 200, and 250 μmol/L group were 99.05%, 96.29%, and 91.20% (Fig. 2A), respectively; after 4 hours, they were 97.18%, 87.17%, and 75.43% (Fig. 2B); and after 6 hours, they were 94.18%, 75.66%, and 60.16% (Fig. 2C). The most significant decrease in the survival rate of KGN cells was observed after treatment with 250 μmol/L H_2O_2 for 6

hours (P<0.001)(Fig. 2D), indicating that the presence of 15% fetal bovine serum affects the results of cell viability detected by the CCK-8 solution. Therefore, serum-free medium was used to prepare the CCK-8 solution in subsequent experiments, and a concentration of 250 μmol/L H_2O_2 with 6 hours treatment was selected for further studies. An optimal cell viability level for inducing apoptosis is approximately 60%, this is consistent with the literature report[18]. If cell viability is excessively high, it may hinder subsequent research.

3.2 Effect of SPPA against apoptosis of KGN cells

Fig. 3A illustrates that during the process of H_2O_2-induced apoptosis, fluorescent probe detected intracellular ROS, showing strong fluorescence intensity after H_2O_2 addition, which was close to the rosup positive control group. The results demonstrated that H_2O_2 could significantly increase intracellular ROS levels. However, after 12 hours of treatment with 50 μg/mL SPPA, the H_2O_2 cells showed improved conditions with a notable decrease in intracellular fluorescence intensity. ROS, NO, MDA, SOD are commonly used indices of lipid oxidation that serve to assess oxidation resistance. As illustrated in Fig. 3B-E, SPPA significantly inhibited the H_2O_2-induced increase in ROS ($P < 0.001$), NO ($P < 0.001$), MDA ($P < 0.05$) levels, while enhancing SOD activity ($P < 0.05$).

The Fig. 4 indicated that compared to the control group, the nuclei of cells in the H_2O_2 group exhibited significant shrinkage of cells and the cell nucleus. The shrunken cell nucleus is brighter (Fig. 4A). In contrast, the nuclei of most cells in the SPPA+H_2O_2 group displayed regular morphology. The statistical analysis of the apoptosis rate revealed that H_2O_2 significantly increased the apoptosis rate of KGN cells, reaching 17% ($P < 0.001$). However, the apoptosis rate declined significantly to 5% after 12 hours of 50

μg/mL SPPA treatment ($P < 0.001$) (Fig. 4B).

The Fig. 5 indicated that compared to the control group, H_2O_2 treatment significantly increased the mRNA expression levels of Caspase-3 ($P < 0.01$) and Bax ($P < 0.001$) (Fig. 5A , C)and decreased the gene expression level of Bcl-2 along with the ratio of Bcl-2 to Bax ($P < 0.05$) (Fig. 5B, D). However, following the addition of 50 μg/mL SPPA treatment, the mRNA expression levels of Caspase-3 ($P < 0.01$) and Bax ($P < 0.001$) were reduced, while the gene expression level of the ratio of Bcl-2 to Bax were elevated ($P < 0.05$).

The protein expression levels were detected by WB, and the results are shown in Fig. 6A. The oxidative stress model of granular cells caused by exposure to H_2O_2 demonstrates significantly lower expression levels of Bcl-2 ($P < 0.05$)and the ratio of Bcl-2 to Bax protein ($P < 0.01$)compared to that of the control group. Treatment with 50 μg/mL SPPA significantly reversed the low Bcl-2 ($P < 0.01$)and the ratio of Bcl-2 to Bax protein expression ($P < 0.01$) (Fig. 6B-C) Moreover, the expression of both Bax and Cleaved-caspase-3/Caspase-3 in the oxidative stress model was also markedly higher than that in the control group ($P < 0.05$). Expressions of Bax and Cleaved-caspase-3/Caspase-3 proteins were downregulated significantly after 50 μg/mL SPPA was added ($P < 0.05$) (Fig. 6D-E).

3.3 Sequencing data quality analysis and sequencing results

To evaluate the quality of sequencing data after the removal of adapters and low-quality sequences from the raw data, we first analyze the average quality distribution of the sample base sequences. As illustrated in Supplementary Fig. S1, the average quality peak value of most base sequences exceeds 30, indicating

that the sequence quality is satisfactory. Next, we examine the base GC content distribution of the miRNA sequences. Supplementary Fig. S2 reveals that there is no discernible separation between base AT and GC content. Finally, we analyze the preference for miRNAs base usage, as shown in Supplementary Fig. S3, which serves as an important criterion for assessing data quality. To eliminate any repeat sequences that may be present in small RNAs (sRNAs), the sRNAs were aligned with the repeat sequences of the species, and the counts of sRNAs corresponding to various repeat types in the alignment were recorded (Supplementary Fig. S4). A statistical analysis was conducted on the length and quantity of the obtained sequences (Supplementary Fig. S5). The typical length of miRNAs is approximately 18 to 24 nt, and the length distribution statistics can be utilized to validate the reliability of the experiment.

The resulting clean reads obtained from the libraries K1, K2, H1, H2, C1, and C2 were 18,059,270; 17,193,880; 18,099,392; 17,594,085; 19,213,136; and 18,331,505, respectively (Table 3). The differential expression of miRNAs, clustering analysis, and target gene function prediction were performed across different samples, and family sequence data from the Rfam database (v 14) were downloaded. The obtained clean data were compared using BLASTN software to analyze the classification of ncRNA within sRNA. The analysis of small RNA composition revealed that miRNAs constituted the largest proportion, accounting for 81.89% (Table 4).

3.4 Analysis of differentially expressed miRNAs

The correlation analysis of sequencing samples indicates that duplicate samples exhibit high similarity and reproducibility, with negligible individual differences, allowing for subsequent analyses

(Fig. 7A). The clustering relationship among the samples is shown in Fig. 7B. A total of 162 differentially expressed miRNAs were identified across three distinct groups (K, H, and C), including 108 candidate novel miRNAs (Supplementary Table 1). A comparison between K and H group revealed 65 miRNAs, of which 30 were upregulated and 35 were downregulated (Fig. 8A). Furthermore, a comparison of H and C groups identified 30 miRNAs, with 19 upregulated and 11 downregulated (Fig. 8B). The intersections of miRNAs between the K vs H and H vs C groups yielded 13 differentially expressed miRNAs (Fig. 8C, Table 5). Expression heatmaps for all differentially expressed miRNAs are presented in Fig. 8D. Functional analysis demonstrated that 5 miRNAs (hsa-miR-378d, NovelmiRNA-1017, hsa-miR-548av-5p, hsa-miR-103a-3p, hsa-miR-6511b-3p) were downregulated in the H_2O_2 group but were upregulated following SPPA-mediated repair(Fig. 8E). Conversely, the remaining 8 miRNAs (NovelmiRNA-72, NovelmiRNA-420, NovelmiRNA-214, NovelmiRNA-383, NovelmiRNA-1063, hsa-miR-548ac, NovelmiRNA-94, NovelmiRNA-881) were upregulated in the H_2O_2 group but downregulated after SPPA treatment (Fig. 8F).

3.5 Target gene prediction and functional annotation of DEMs

To better understand the function of miRNAs regulated by SPPA in KGN cells following oxidative stress, we analyzed 13 differentially expressed miRNAs. Among these 6 DEMs (NovelmiRNA-881, hsa-miR-548ac, NovelmiRNA-94, NovelmiRNA-1063, NovelmiRNA-1017 and hsa-miR-548av-5p) did not predict target genes. The remaining 7 DEMs predicted a total of 3534 target genes, which were subsequently analyzed for enrichment in GO and KEGG pathways. We selected 30

significantly enriched items for GO analysis (Fig. 9), encompassing molecular function (MF), cellular component (CC), and biological process (BP) categories. These target genes are crucial in the anti-apoptotic process. The BP category primarily highlights the enrichment of terms related to cysteine endopeptidase activity involved in cytC activation and apoptosis, positive regulation of cell proliferation, positive regulation of intrinsic apoptosis signaling pathways, and transcription initiation at the RNA polymerase II promoter. The CC predominantly include the lysosomal membrane, cytoplasm, and nucleus. In terms of MF, the targets are mainly enriched in DNA-directed 5'-3' RNA polymerase activity, RNA polymerase II complex binding, and binding to DNA and RNA.

As shown in Fig. 10, the target genes of 13 DEMs are enriched in multiple KEGG pathways (Fig. 10A), primarily within the two branches of cellular processes and environmental information processing (Fig. 10B). Among these notable pathways, several are intricately involved in the process of cell apoptosis, including apoptosis, metabolic pathways, lysosomal pathways.

3.6 MiRNA-mRNA regulatory network

To elucidate the targeting relationships of differentially expressed miRNAs across various functional clusters and pathways, we retrieved multiple target genes involved in regulating KGN cells apoptosis from both GO and KEGG analysis results, as well as from published literature. Subsequently, we constructed a miRNA-mRNA interaction network (Fig. 11A). This network reveals that miRNAs regulate multiple target genes that interact with one another, rather than focusing on a single target. They exert a regulatory role by coordinating the activities of genes across various biological functions, thereby indirectly or directly influencing the expression of multiple genes.

3.7 QPCR verification of candidate miRNAs

To further validate the differentially expressed miRNAs identified through miRNA-seq, we randomly selected 5 miRNAs for qPCR validation (Fig. 11B). Notably, NovelmiRNA-214 and NovelmiRNA-383 were significantly upregulated following H_2O_2 treatment compared with the control group, while their expression was downregulated in the group treated with SPPA (following H_2O_2 treatment) relative to the H_2O_2-treated group. Conversely, compared to the control group, H_2O_2 treatment significantly downregulated expression of hsa-miR-103a-3p, hsa-miR-378d and NovelmiRNA-1017, while their expression was upregulated in the group treated with SPPA relative to the H_2O_2-treated group. The qPCR results were consistent with those obtained from miRNA-seq analysis.

4. Discussion

POF is a common disease in women at childbearing age, and it is a common gynecological secretory disease[19]. It's worth noting that all POF will induce oxidative stress in the early stages, thus producing apoptosis of granular cells[20]. Some studies focused on oxidative stress closely related to apoptosis of granular cells[21,22]. Mammalian cells always integrate and respond to stress stimuli to decide cell fates whether to survive or die on a continuous basis. Several genes and signaling pathways are involved in this decision-making. As a master regulator of gene expression, miRNAs may play a significant role in this very complex mechanism. However, The mechanism that miRNA regulates apoptosis remains unclear. H_2O_2 has been used as an oxidant in several studies and proves that it causes excess ROS generation and induces GCs apoptosis in vivo[23]. Oxidative stress (H_2O_2) hinders development of

follicle[24] by inducing apoptosis of granular cells and causes POF by lowering the ovarian reserve function[25]. Importantly, miRNAs have been shown to be the major mediators affecting cell function under conditions of oxidative stress[26,27]. In the present study, our findings indicate that the presence of 15% fetal bovine serum significantly increase the results of cell viability assays conducted using the CCK-8 solution. Therefore, preparing the CCK-8 solution with a serum-free medium and treating cells with a concentration of 250 μmol/L H_2O_2 for 6 hours induced ROS generation and oxidative stress in GCs, which subsequently induced apoptosis in KGN cells and inhibited cell viability. According to DAPI specific dyeing of cell nucleus, karyopyknosis phenomenon can be seen clearly through a fluorescence microscope. Generally, apoptosis cell nucleus shows obvious pyknosis and pyknotic cell nucleus represent apoptosis cells[28]. Caspase-3, Bax and Bcl-2 are the recognized cell apoptosis genes and their appearance represents that cells are having apoptosis[29]. Detection results of ROS, NO, MDA, and SOD levels, DAPI specific dyeing and Caspase-3, Bax and Bcl-2 mRNA and protein expression analysis show that SPPA repairs KGN cells after apoptosis significantly.

A previous study using high-throughput sequencing technology showed that oxidative stress modulates the expression of miRNAs in bovine GCs[30]. Furthermore, a study reported that the PA significantly reduces the expression of miR-29a in mice with ulcerative colitis (UC), increases the expression of PTEN protein, and inhibits the protein expression of the PI3K/AKT/mTOR pathway. By regulating the miR-29a/PTEN/PI3K axis to restore the homeostasis of Treg cells, this extract may be utilized to treat ulcerative colitis[31]. However, there are no reports on the anti-apoptotic function of SPPA being exerted through the

regulation of miRNA. We employ high-throughput sequencing technology for miRNAs to predict target genes of miRNAs and screen for DEMs in groups. In the present studies, we focus on the miRNA expression profiles associated with SPPA inhibition of KGN cells apoptosis, and a total of 13 DEMs were discovered. Among them, miR-103a-3p, miR-214, and miR-383 play important roles in the regulation of apoptosis.

Altered levels of miR-214 in tumors seem to hint at a possible influence on proliferation and cell cycle control; however, existing data are controversial[32]. It has been reported that this miRNA targets uncoupling protein 2 (UCP2), significantly reducing oxidative stress and levels of ROS[33]. Additionally, it has been showed that miR-214 enhances cell survival and inhibits apoptosis; furthermore, the inhibition of miR-214 negates its protective effects, compromising cell survival and anti-apoptotic mechanisms[34]. However, The study demonstrated that ectopic expression of miR-214 reduces cell survival, induces apoptosis and enhances sensitivity to cisplatin through directly inhibiting Bcl2l2 expression in cervical cancer HeLa and C-33A cells[35]. Further investigations revealed that miR-214-3p directly regulated ABCB1 and XIAP expression to promoted cell apoptosis in vitro and in vivo[36]. Literature research indicated that miR-214 promotes apoptosis by targeting the RFWD2-p53 cascade[37]. Some of these studies are consistent with our research results. In this study, the expression of miR-214 was found to be upregulated in the H_2O_2 group compared to the control group. Following treatment with SPPA, the expression level of miR-214 was downregulated, this suggest that miR-214 may be associated with apoptosis. SPPA may exert an anti-apoptotic effect through miR-214. However, whether miR-214 ultimately promotes or inhibits apoptosis depends entirely on the

cellular context in which it resides and the specific network of target genes it regulates. Besides, there are limitations to using bioinformatics to predict target genes and thereby regulate biological effects.

MiR-103a-3p was first discovered in human cervical cancer HeLa cell line, and its abnormal expression is closely related to ovarian diseases. Huang et al[38] found that miR-103a-3p may be involved in the functional regulation of granulosa cells by affecting the proliferation and apoptosis of granulosa cells, thus affecting polycystic ovary syndrome (PCOS). It has reported that interfering with miR-103a-3p is able to inhibit Lipopolysaccharide (LPS) -induced hepatocyte apoptosis, inflammation and oxidation reactions[39]. Zhang et al[40] reported that miR-103a-3p exerted negative influences on the maturation of oocytes by regulating brain-derived neurotrophic factor (BDNF) expression in human follicular fluid. However, Cheng et al[41] found that upregulation of miR-103a-3p promoted chondrocyte proliferation of human osteoarthritis and inhibited cell apoptosis and inflammatory responses. Furthermore, signal transducer and activator of transcription 1 (STAT1) is a potent growth inhibitor and apoptosis promoter, exhibiting a significant regulatory role in tumor development. As reported by Benco et al[42] that STAT1 is involved in the regulation of apoptosis, proliferation and secretion in ovarian GCs. In our study, we observed that miR-103a-3p was upregulated following SPPA repair, which targets STAT1 and subsequently inhibits apoptosis. Although there is no direct literature reporting that miR-103a-3p targets STAT1 to inhibit apoptosis, our study provides a possible outcome.

The studies have demonstrated that miR-383 functions as a tumor suppressor in various cancer[43]. MiR-383 induces apoptosis

in nude mouse cells and inhibits cell viability and tumorigenicity by modulating the Wnt/β-catenin signaling pathway[44]. Additionally, research has shown that miR-383 downregulates cell cycle-related protein scyclin D1, cyclin B, cyclin-dependent kinase 1, 2, 4 (CDK1, CDK2, CDK4), effectively inhibiting the proliferation of mouse granulosa cells by blocking the G0/G1 phase[45], which also was observed in our study. We found that miR-383 targeted cell cycle genes, such as cyclin-dependent kinase 6 (CDK6), cyclin L1 (CCNL1), and cell division cycle 6 (CDC6), were upregulated following H_2O_2 treatment, which inhibited cell proliferation. Moreover, overexpression of miR-383-5p has been found to inhibit the proliferation and invasion of glioma cells while promoting cell apoptosis[46]. MiR-383-5p induces apoptosis by downregulating cold inducible RNA-binding protein (CIRP) protein expression in KGN cells and inhibiting signaling within the PI3K/AKT pathway[47]. This suggests that it has also been studied in KGN cells, and our findings are consistent with it. Our research indicates that miR-383 targets anti-apoptotic gene nuclear factor (erythroid-derived 2)-like 2 (NFE2L2) and manganese superoxide dismutase (SOD2) for inhibition, thereby exerting a pro-apoptotic effect in KGN cells. Interestingly, our research also reveals that miR-383 can target pro-apoptotic proteins, including BH3 interacting domain death agonist (Bid), Bcl-2-associated X protein gene (Bax), cysteine-aspartate specific protease 8, 9 (CASP8, CASP9). These results indicate that miRNAs can target multiple genes to regulate various biological processes across different cell types. It is worth noting that target genes AGO1 and AGO3 (miRNA-processing enzyme encoding genes) of miR-383 were significantly upregulated during SPPA repair, which may partially explain the multiple

miRNAs differentially expressed in KGN cells undergoing oxidative stress.

Additionally, this study derived the biological functions of 3534 target genes of the aforementioned 13 DEMs through GO functional annotation and KEGG pathway enrichment analysis. The enrichment analysis of signaling pathways confirms that these target genes are significantly enriched in metabolic pathways and lysosomes. In their investigation of key genes involved in resveratrol-induced apoptosis in porcine ovarian granulosa cells, Zhang et al[48] identified that the significantly enriched pathways were associated with hormone secretion and metabolic pathways. Furthermore, it has been examined that the expression profiles of miRNAs in the ovaries of rats with insulin-resistant PCOS and discovered that the predicted target genes were correlated with metabolic pathways, with these pathways being the most enriched in the KEGG analysis[49], aligning with our findings. Research has indicated that granulosa cells can function as a barrier, protecting oocytes from the extra-ovarian microenvironment through metabolic and signaling interactions. Lin et al[50] observed significant alterations in the transcriptional activity of genes related to neuroactive ligand-receptor interactions and metabolic pathways in mice with premature ovarian failure, suggesting that metabolic pathways may play a crucial role in this condition. A prior study reported that women with PCOS experience fertility changes primarily linked to metabolic disorders, such as insulin resistance, hyperinsulinemia, and dyslipidemia[51]. This correlation underscores the importance of metabolic pathways in regulating the reproductive system.

Lysosomes are vital for cell survival as they can eliminate injured, oxidized, or dysfunctional organelles within cells. The

initial reports regarding lysosomal destabilization or lysosomal membrane permeability (LMP) as an early event in apoptosis emerged approximately thirty years ago. This discovery resulted from experiments investigating the induction of apoptosis in cultured cells through moderate oxidative stress. It was observed that LMP occurred as a response to this stress, which was subsequently followed by mitochondrial membrane permeability (MMP) and classical apoptosis[52]. Several studies have indicated that lysosomal metabolic pathways and the signaling pathways of various lysosomal proteases play significant roles in the apoptosis process. Furthermore, it has been reported that in apoptosis models, lysosomal membrane transparency occurs early in the apoptotic process, suggesting that this may be a key factor contributing to apoptosis and apoptotic cell death[53]. Although the expression profiles of miRNA were discussed and multiple differentially expressed miRNAs were verified by qPCR in the present study, further studies are required to support the results in vitro. Moreover, the mechanisms underlying the differential expression of miRNAs in response to SPPA, which mitigate apoptosis induced by oxidative stress, as well as the impact of their interaction network on the state and function of KGN cells, require more precise elucidation in future studies.

5 Conclusion

In summary, we constructed differentially expressed miRNA profiles using miRNA-seq technology in this study and demonstrated that dramatic changes in miRNA expression occurred in KGN cells under oxidative stress and SPPA repair. Based on the analysis of miRNAs functions and KEGG enrichment pathways, the involvement of miRNAs molecules and their action pathways in SPPA resistance to H_2O_2-induced cell apoptosis has

been fundamentally interpreted. This research offers a new perspective on studying SPPA treatment of POF at the miRNAs level. Importantly, this study provides novel insights suggesting that further investigations into the potential roles of *Periplaneta americana* in the human reproductive system, particularly concerning the regulatory mechanisms of hsa-miR-103a-3p, NovelmiRNA-214 and NovelmiRNA-383 may yield significant outcomes (Fig. 12). The integrated analysis of miRNA-mRNA interaction networks also provides a series of potential therapeutic targets for oxidative stress-induced female infertility.

Author contributions

Linjie Xu: conceptualization, data curation, methodology, project administration, resources, software, supervision, validation, writing-original draft. **Rong Jiang:** data curation, formal analysis, investigation, methodology, resources, software, validation, writing-original draft. **Jingjing Su:** data curation, investigation, resources, visualization, writing-review & editing. **Ruixian Sun:** formal analysis, methodology, resources, supervision, writing-original draft. **Lilian Yang:** formal analysis, project administration, resources. **Yunping Tang:** formal analysis, resources. **Shiyan Sui:** conceptualization, funding acquisition, project administration, resources, supervision, validation, writing-review & editing. All authors have read and agreed to the published version of the manuscript.

Funding

This work was supported by National Natural Science Foundation of China (NO. 32260865); Yunnan Province Young and Middle-aged Academic and Technical Leaders Reserve Talents Project (NO. 202305AC160037), Wang Junjun Expert Workstation Project of Yunnan Province (NO. 202305AF150083); Basic

Research Program of Yunnan Provincial Department of Science and Technology (NO. 202101BA070001-202).

Ethics approval

The authors confirm that this study received approval from the relevant institutional and/or national research ethics committee, specifically the Medical Ethics Committee of Dali University, under the ethics approval number MECDU-202110-4.

Declaration of competing interest

The authors declare that they have no known competing financial interests or personal relationships that could have appeared to influence the work reported in this paper.

Acknowledgements

We would like to thank Suzhou Jinweizhi Biotechnology Co., Ltd for miRNA-seq data analysis. Additionally, thanks to figdraw (https://www.figdraw.com/static/index.html#/) for providing the drawing platform and everyone who was involved in this study.

Data availability

The miRNA-seq raw data is deposited on the Sequence Read Archive (SRA) database at https: //www.ncbi.nlm.nih.gov/bioproject, BioProject: PRJNA837735.

Table 1 The primer sequences of genes

Genes	Primer sequence (5′–3′)
Caspase3	F: GTGGAGGCCGACTTCTTGTATGC
Caspase3	R: TGGCACAAAGCGACTGGATGAAC
Bax	F: GATGCGTCCACCAAGAAGCTGAG
Bax	R: CACGGCGGCAATCATCCTCTG
Bcl-2	F: TACGAGTGGGATGCGGGAGATG

Bcl-2	R: CCGGGCTGGGAGGAGAAGATG
β-actin	F: TGACAACAGCCTCAAGAT
β-actin	R: GAGTCCTTCCACGATAC

Table 2 Information of miRNA primers

miRNA	Primer sequence （5'→3'）
NovelmiRNA-383	TCTGGGCAGCAAAGTGAGACC
NovelmiRNA-214	ATATGATTACCTCGCTGGGGC
hsa-miR-378d	CCGACTGGACTTGGAGTCAGAAA
hsa-miR-103a-3p	ACGACGAGCAGCATTGTACA
NovelmiRNA-1017	GCCGAGGACTTGTCTTAGGTGT

Table 3 Analysis of KGN cell sequencing data in groups K, H and C

Sample	Average length	Raw reads	Clean reads	Q20 (%)	Q30 (%)	GC (%)
K1	22.42	24572529	18059270	99.35	97.39	44.33
K2	22.32	24734510	17193880	99.41	97.68	43.87
H1	22.31	24036389	18099392	99.37	97.58	44.56
H2	22.61	22027661	17594085	99.38	97.51	44.02
C1	22.45	25604876	19213136	99.33	97.46	44.13
C2	22.45	24355124	18331505	99.28	97.38	44.57

Q20,Q30: The ratio of bases with Phred quality scores exceeding 20 and 30 to the total number of bases is analyzed. A higher Phred score indicates a lower sequencing error rate (e), ideally maintained below 0.5%. Additionally, GC(%): GC content is expressed as the percentage of guanine (G) and cytosine (C) bases relative to the total number of bases sequenced.

K: control group H: H_2O_2 group C: H_2O_2+SPPA group

Table 4 Small RNA composition analysis results of 2 repeated samples in groups K, H and C

sample	K1	K2	H1	H2	C1	C2	Percentage
miRNA	11433150	10894080	11470833	11529199	12992422	12297226	81.89%
rRNA	263308	292912	270963	298385	198546	217787	1.79%
snRNA	67902	62663	64587	63786	68287	64787	0.45%
snoRNA	191839	159059	162194	221701	213801	209601	1.34%
tRNA	195550	163739	182417	202393	166471	174459	1.26%
others	1835220	1738691	1970848	1913859	2023117	1960217	13.27%

K: control group H: H_2O_2 group C: H_2O_2+SPPA group

Table 5 DE miRNAs related information

miRNA Name	**log_2FoldChange**	***P value***	**log_2FoldChange**	***P value***	**Regulation**
	(K VS H)		**(H VS C)**		
NovelmiRNA-881	8.44	0.01	-8.52	< 0.01	Up-Down
NovelmiRNA-214	9.51	0.01	-9.60	0.01	Up-Down
NovelmiRNA-420	9.39	0.01	-9.48	0.01	Up-Down
NovelmiRNA-72	9.39	0.01	-9.48	0.01	Up-Down
hsa-miR-548ac	8.62	0.03	-8.69	0.03	Up-Down
NovelmiRNA-94	8.61	0.03	-8.68	0.03	Up-Down
NovelmiRNA-383	8.58	0.03	-8.65	0.03	Up-Down
NovelmiRNA-1063	8.33	0.05	-8.42	0.04	Up-Down
hsa-miR-103a-3p	-20.21	< 0.01	19.28	< 0.01	Down-Up
NovelmiRNA-1017	-16.30	< 0.01	15.16	< 0.01	Down-Up
hsa-miR-548av-5p	-9.18	< 0.01	8.35	< 0.01	Down-Up
hsa-miR-6511b-3p	-8.76	< 0.01	7.96	0.02	Down-Up
hsa-miR-378d	-8.78	0.02	8.53	0.04	Down-Up

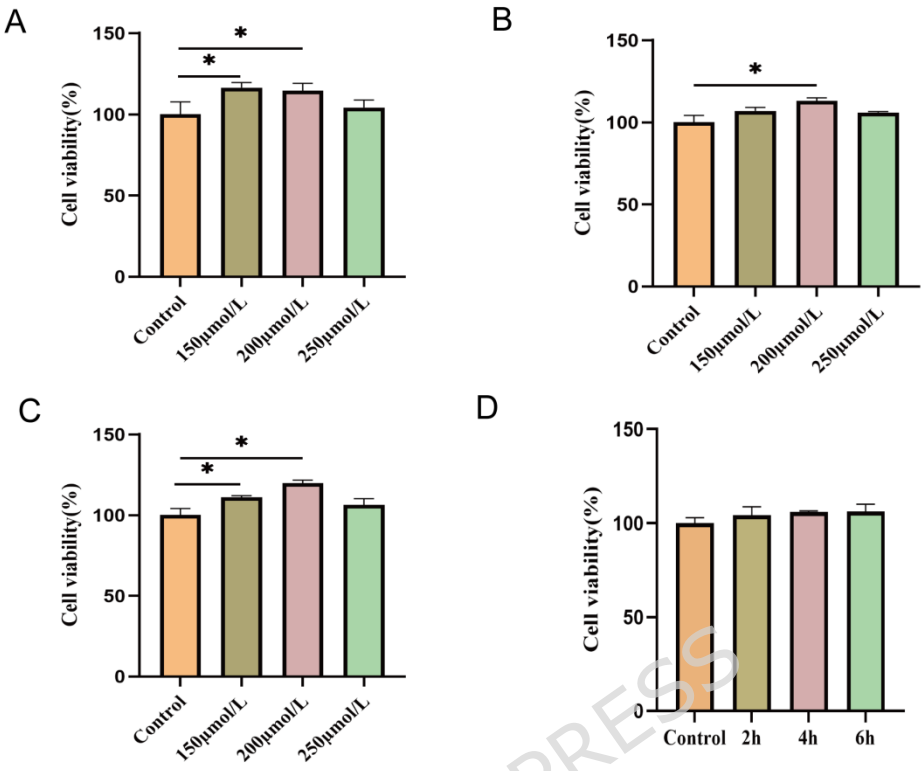

Fig. 1. Comparison of cell activity in different H_2O_2 concentrations treated at different time points. To prepare for the CCK-8 assay, 15% fetal bovine serum was added to the culture medium.(A) Cells were treated with H_2O_2 (0, 150, 200, 250μmol/L) for 2h. (B) Cells were treated with H_2O_2 (0, 150, 200, 250μmol/L) for 4h. (C) Cells were treated with H_2O_2 (0, 150, 200, 250μmol/L) for 6h. (D) Cells were treated with 250 μmol/L H_2O_2 at different time. *$P < 0.05$

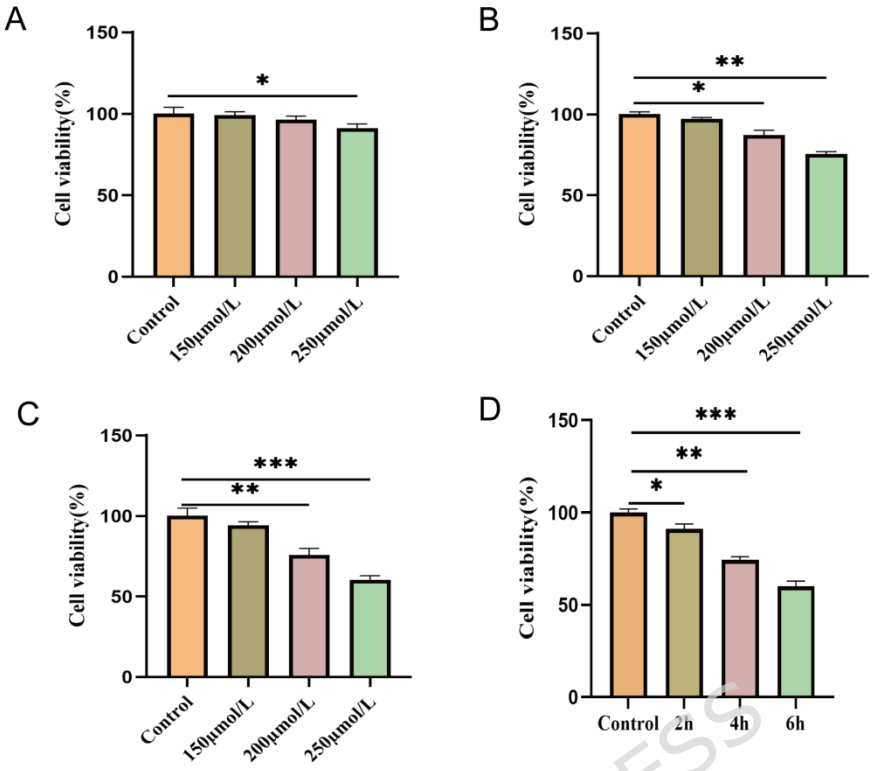

Fig. 2. Comparison of cell activity in different H_2O_2 concentrations treated at different time points. To prepare for the CCK-8 assay, serum-free medium was added to the culture medium.(A) Cells were treated with H_2O_2 (0, 150, 200, 250μmol/L) for 2h. (B) Cells were treated with H_2O_2 (0, 150, 200, 250μmol/L) for 4h. (C) Cells were treated with H_2O_2 (0, 150, 200, 250μmol/L) for 6h. (D) Cells were treated with 250 μmol/L H_2O_2 at different time. *P < 0.05, **P < 0.01, ***P < 0.001.

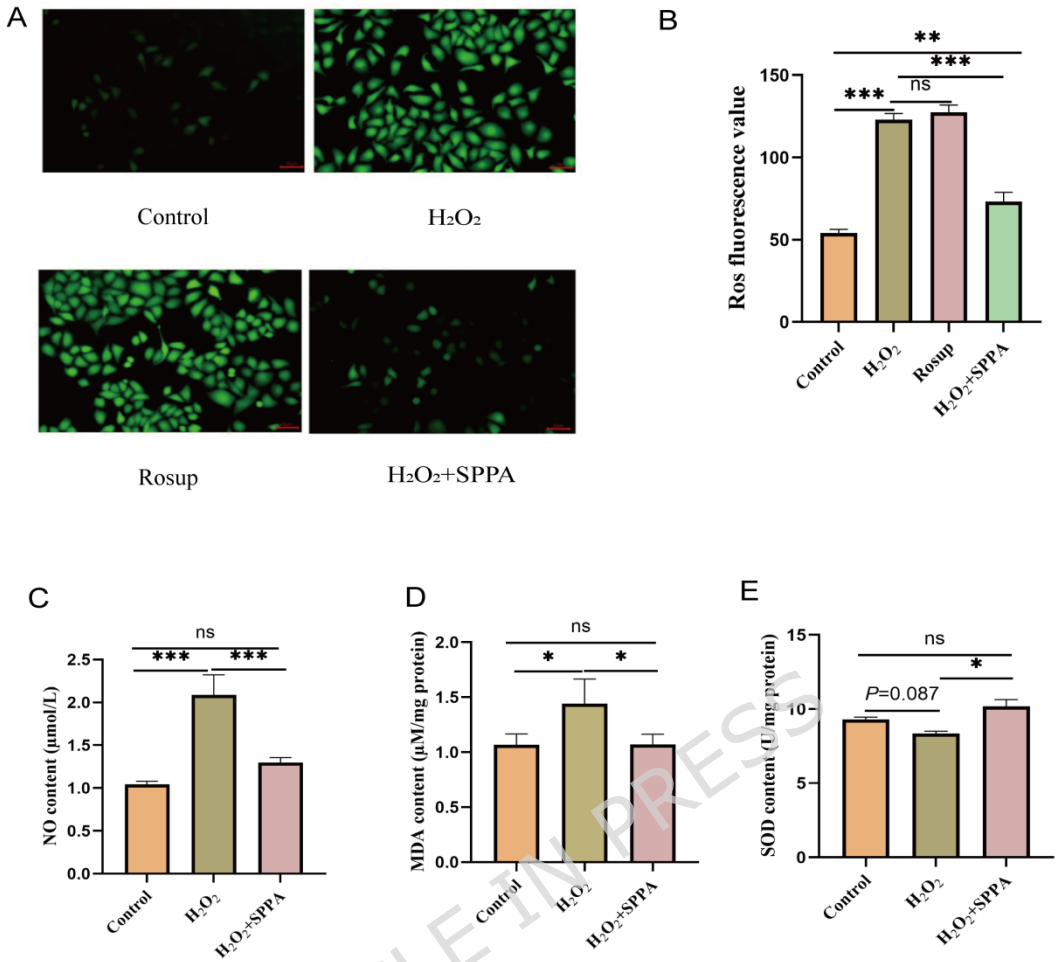

Fig. 3. The ability of 50 μg/mL SPPA for 12h against oxidative stress of granulosa cells. (A) Detection of reactive oxygen species (ROS) by fluorescent probe DCFH-DA (200×, scale bars = 50 μm). Rosup group, positive control reagent for reactive oxygen species. (B) Comparison of ROS fluorescence value after H_2O_2 cells treated by SPPA. (C) Comparison of NO content after H_2O_2 cells treated by SPPA (n = 4). (D) Comparison of MDA content after H_2O_2 cells treated by SPPA (n = 4). (E) Comparison of SOD content after H_2O_2 cells treated by SPPA (n = 4). $^*P < 0.05$, $^{**}P < 0.01$, $^{***}P < 0.001$.

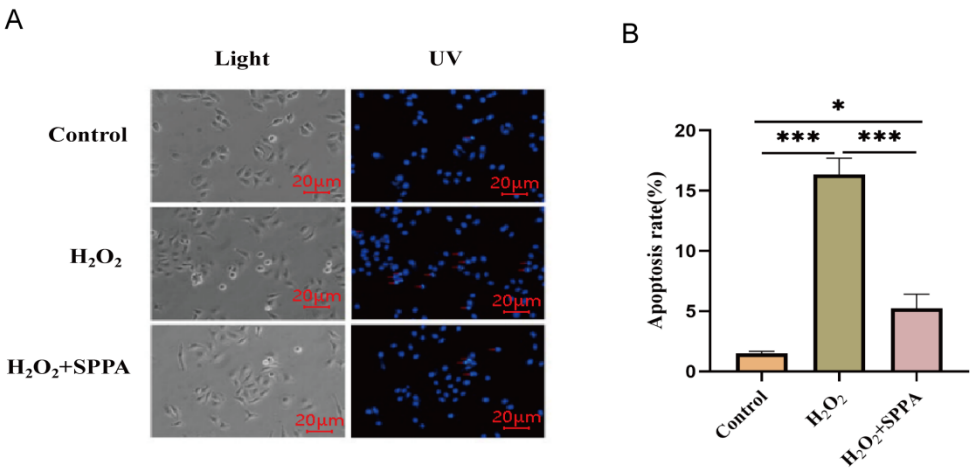

Fig. 4. Cell apoptosis was measured by DAPI (4′,6-diamidino-2-phenylindole) staining. (A) The cell states of control group, H_2O_2 group, and H_2O_2+SPPA group, were examined under white light and ultraviolet fluorescence using a fluorescence microscope (scale bars = 20 μm). (B) Comparison of apoptosis rates among each group of cells. $^*P < 0.05$, $^{***}P < 0.001$.

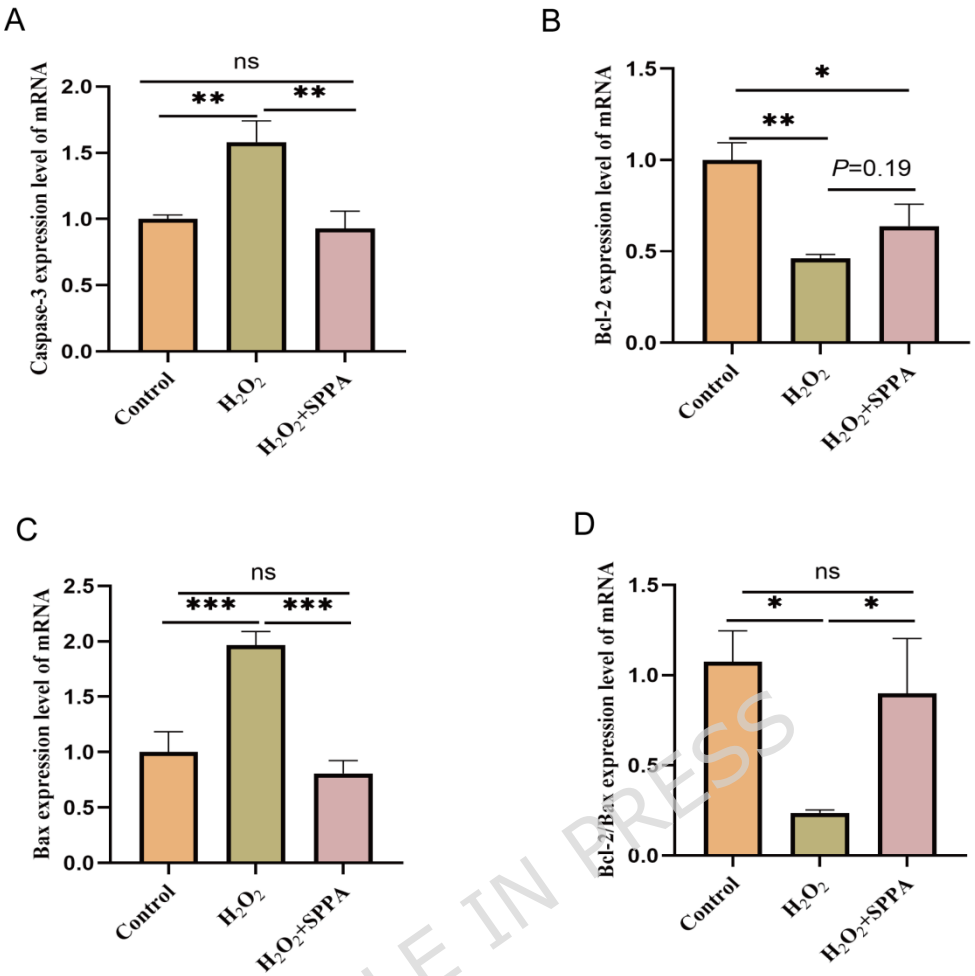

Fig. 5. Treatment effect of 50 μg/mL SPPA for 12h on H_2O_2-induced apoptosis of KGN cells. (A) MRNA level of Caspase-3 in KGN cells (n = 4). (B) MRNA level of Bcl-2 in KGN cells (n = 4). (C) MRNA level of Bax in KGN cells (n = 4). (D) MRNA level of Bcl-2/Bax in KGN cells. *$P < 0.05$, **$P < 0.01$, ***$P < 0.001$.

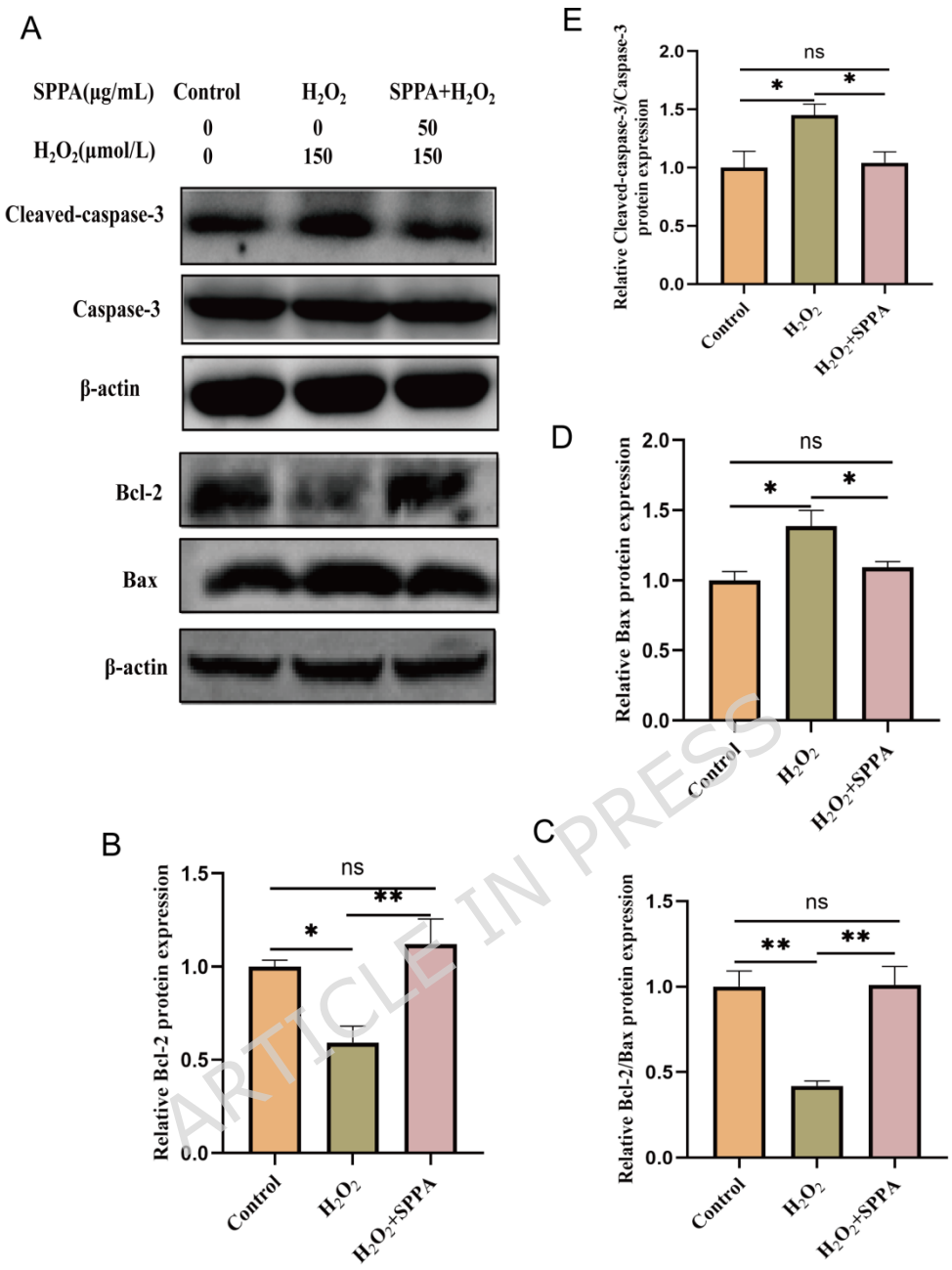

Fig. 6. Anti-apoptotic effects of 50 μg/mL SPPA for 12h. (A) Gel electrophoresis pattern of Cleaved-caspase-3, Caspase-3, Bcl-2, and Bax Proteins (n = 3). Effects of SPPA on the expression level of (B) Bcl-2 protein, (C)the ratio of Bcl-2 to Bax protein (D) Bax protein and (E) the ratio of Cleaved- caspase-3 to Caspase-3 protein. *$P < 0.05$, **$P < 0.01$.

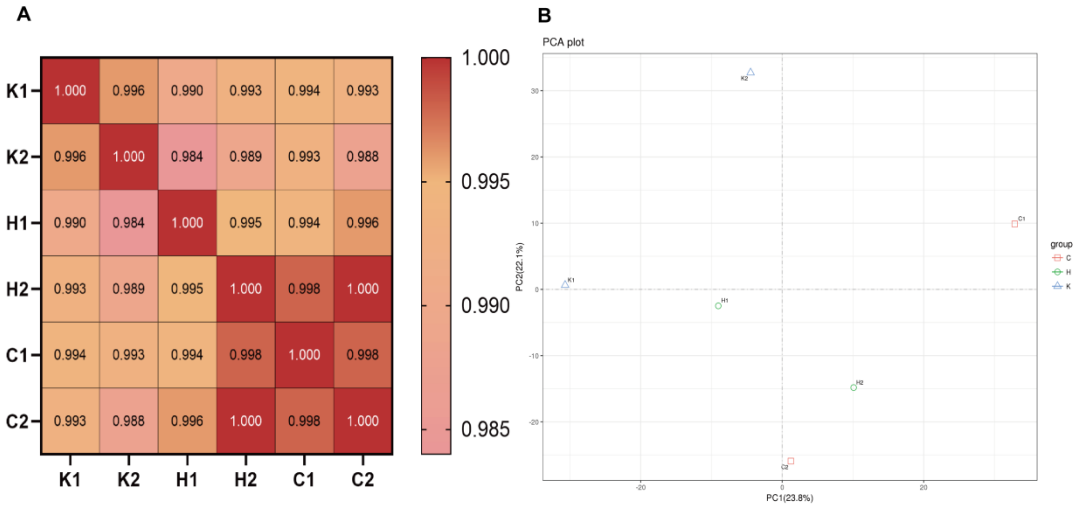

Fig. 7. Visualization of transcriptome analysis results among the K, H, and C groups. (A) the correlation between sequencing samples; values closer to 1 in the grid indicate a stronger correlation. (B) Principal component analysis (PCA) plot (PC1 = 23.8%; PC2 = 22.1%). The position of each point represents the value of the sample in each principal component.

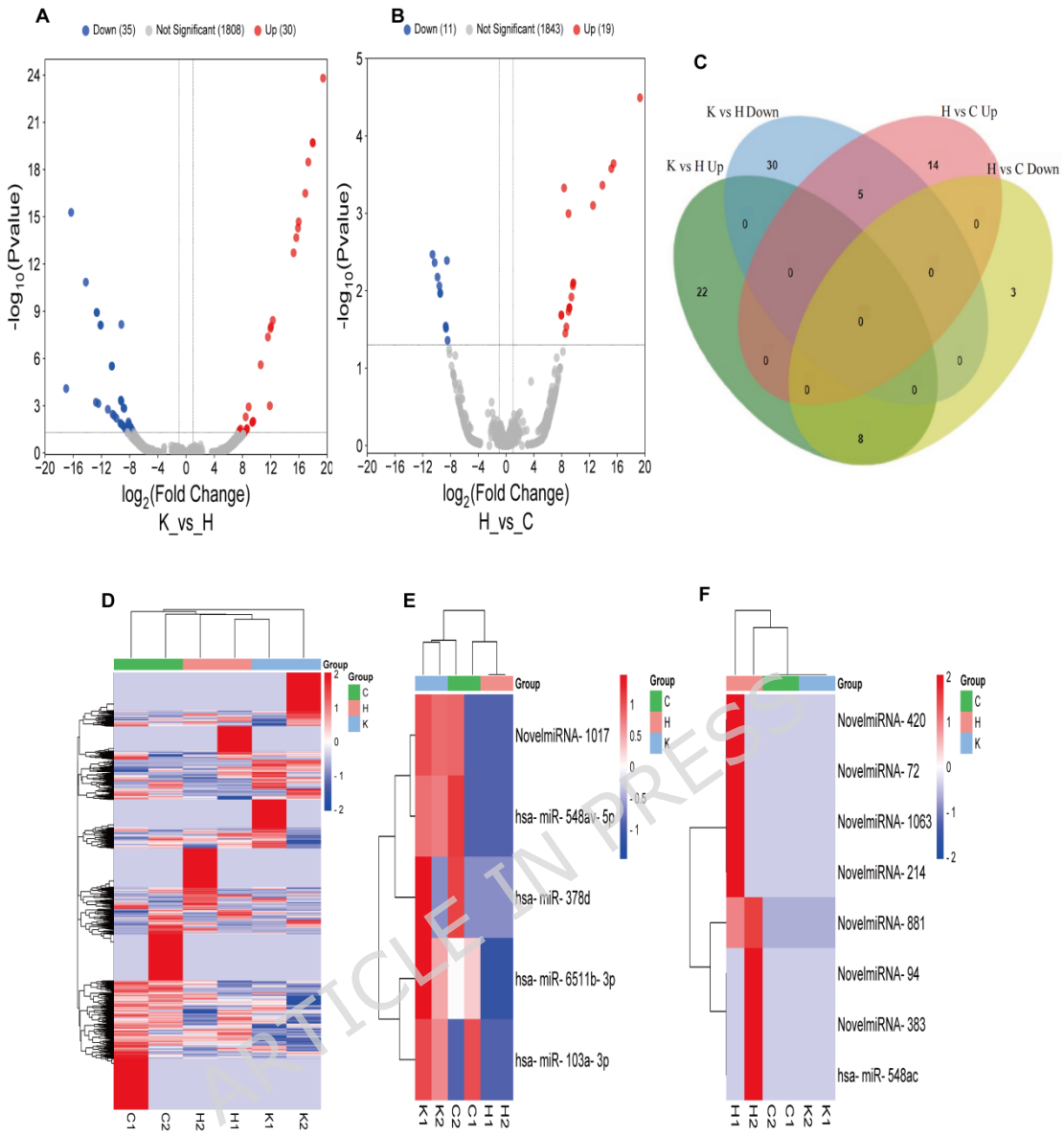

Fig. 8. MiRNA expression profiles among the K, H, and C groups, analyzed using miRNA-seq. (A, B) The volcano plot of differentially expressed miRNAs, where red dots represent significantly upregulated miRNAs and blue dots denote significantly downregulated miRNAs. (C) A Venn diagram of overlapping miRNAs. (D, E, F)The cluster heat map of the differential expression of miRNAs based on $\log_2$(CPM), with blue indicating low expression and red indicating high expression. The color gradient from blue to red signifies increasing miRNA expression.

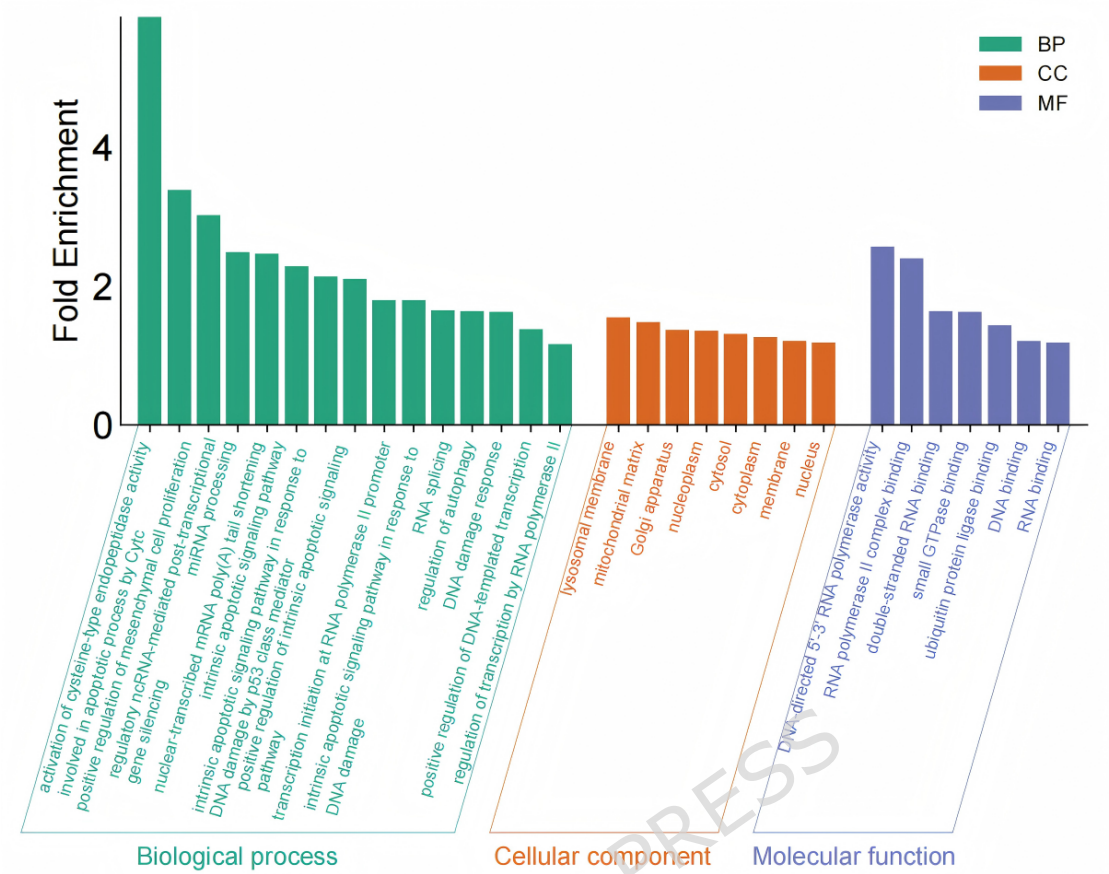

Fig. 9. Gene Ontology (GO) analysis of 13 overlapping differentially expressed target genes of miRNAs. The X-axis displays the names of the GO terms associated with these target genes, while the Y-axis indicates the fold enrichment for each GO term. A higher fold enrichment value signifies a greater degree of enrichment of the target genes under the experimental conditions. GO terms with $P < 0.05$ were considered as significantly enriched.

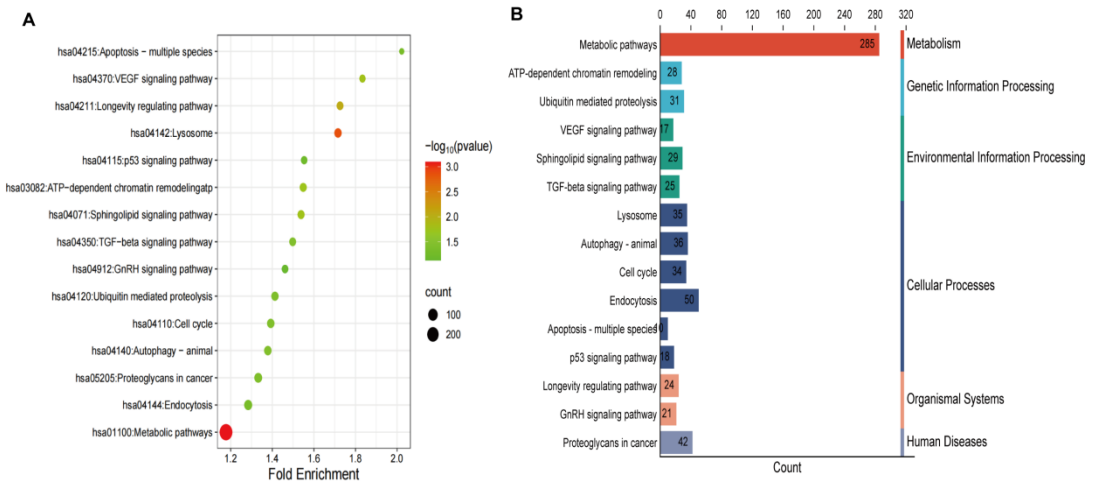

Fig. 10. KEGG enrichment analysis of 13 overlapping miRNAs. (A) The first 15 significantly enriched signaling pathways are displayed, with the X-axis representing the gene enrichment multiple and the Y-axis indicating the pathway names. The size of each circle corresponds to the number of genes enriched in the pathway; larger circles indicate a greater number of genes enriched. (B) Classification diagram of KEGG pathway enrichment results. KEGG pathway terms with $P < 0.05$ were considered as significantly enriched.

The citation guidelines: www.kegg.jp/kegg/kegg1.html. For previous uses, the Kanehisa laboratory have happily provided permission.

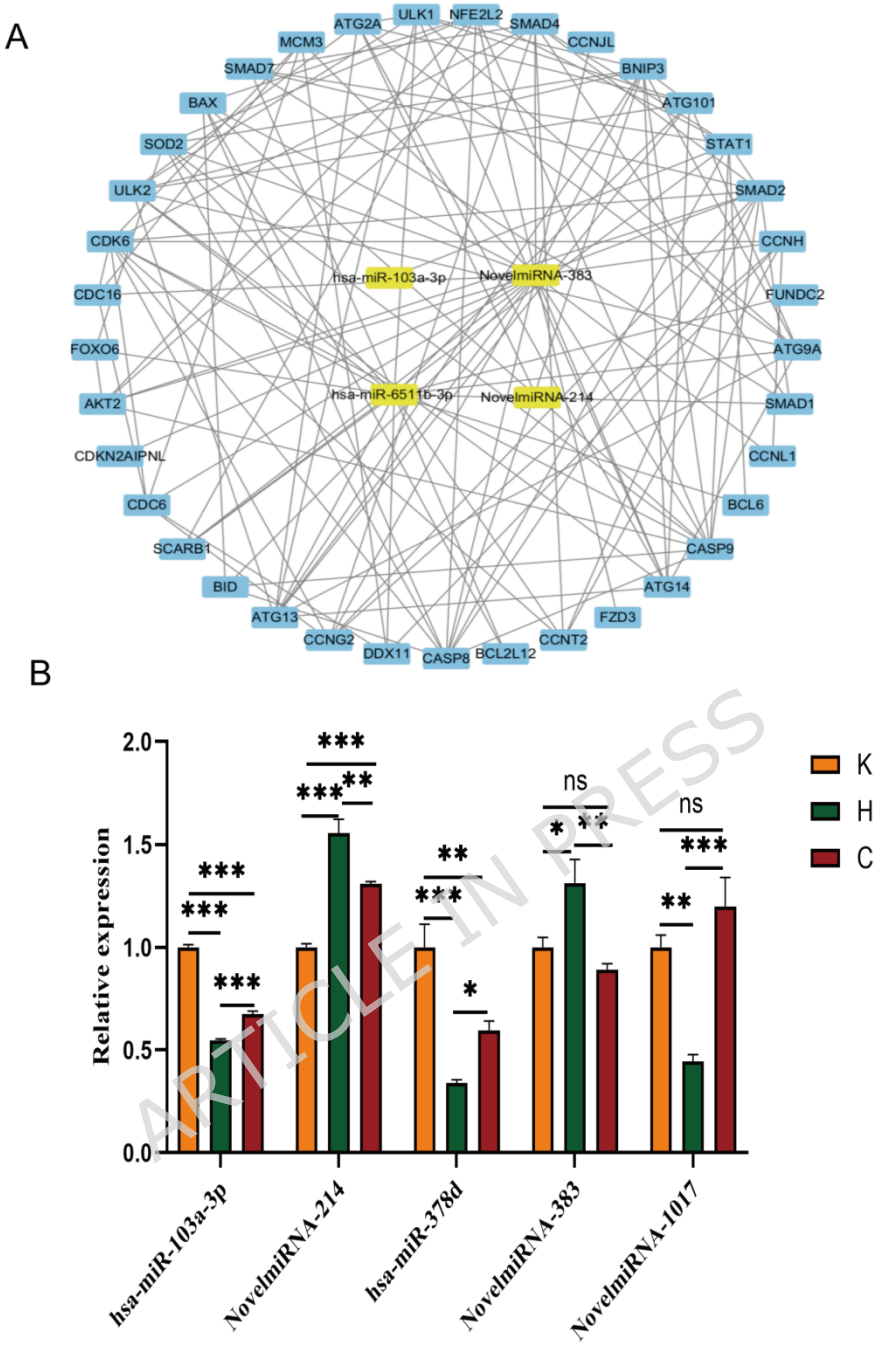

Fig. 11. MiRNA-mRNA interaction network along with real-time quantitative PCR (qPCR) validation. (A) presents a network diagram depicting the targeted regulation of mRNA by miRNA, as well as the interactions between different mRNAs. (B) qPCR verification of expression modes of 5 DEMs in different groups (n = 4). The data are expressed as mean ± SEM. *$P < 0.05$, **$P < 0.01$, ***$P < 0.001$.

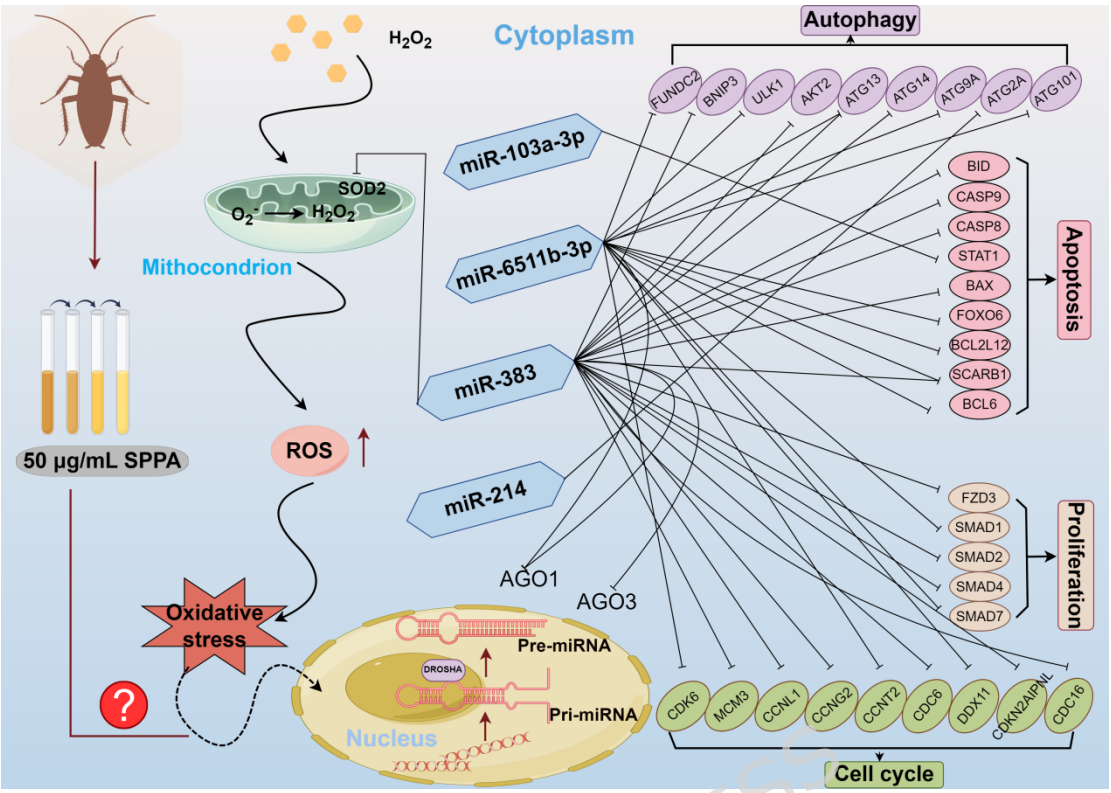

Fig. 12. Model of the resistance of small peptides from *periplaneta americana* (SPPA) to H_2O_2-induced Apoptosis in ovarian granules cells (KGN cells). Exogenous hydrogen peroxide induces ROS production and accumulation in KGN cells to trigger oxidative stress, and SPPA inhibits this process significant changes in the transcriptome. A network of known or predicted DEmiRNA-mRNA functional interactions in KGN cells after experiencing oxidative stress and repaired by SPPA are demonstrated. Hexagons represent DEmiRNA and ellipticals represent mRNA. In addition, multiple important factors involved in cell autophagy, apoptosis and proliferation and cell cycle are differentially expressed after SPPA resistance to H_2O_2-mediated oxidative stress. ↓: Promote ⊥: Inhibit □: Regulate

Note: The use of solid lines to connect miRNAs and target genes does not imply that all target genes have been experimentally validated in the context of the disease or

system; rather, it indicates that these target genes were predicted using the Miranda software.

References

1. Golezar, S., Ramezani, T. F., Khazaei, S., Ebadi, A. & Keshavarz, Z. The global prevalence of primary ovarian insufficiency and early menopause: a meta-analysis. *Climacteric* **22**(4), 403-411 (2019).
2. Liang, Q. X. et al. Ablation of beta subunit of protein kinase ck2 in mouse oocytes causes follicle atresia and premature ovarian failure. *Cell Death Dis.* **9**(5), 508 (2018).
3. Hussein, M. R. Apoptosis in the ovary: molecular mechanisms. *Hum. Reprod. Update* **11**(2), 162-177 (2005).
4. Tiwari, M. et al. Apoptosis in mammalian oocytes: a review. *Apoptosis* **20**(8), 1019-1025 (2015).
5. Agarwal, A., Gupta, S. & Sharma, R. K. Role of oxidative stress in female reproduction. *Reprod. Biol. Endocrinol.* **3**, 28 (2005).
6. Zhang, H. et al. Periplaneta americana extract used in patients with systemic inflammatory response syndrome. *World J. Emerg. Med.* **7**(1), 50-54 (2016).
7. Zhao, B. et al. Periplaneta americana extract promotes hard palate mucosal wound healing via the pi3k/akt signaling pathway in male mice. *Arch. Oral Biol.* **158**, 105856 (2024).
8. Kong, C. et al. Periplaneta americana peptide decreases apoptosis of pig-ovary granulosa cells induced by h(2) o(2) through foxo1. *Reprod. Domest. Anim.* **56**(11), 1413-1424 (2021).
9. Fu, R. et al. Small peptides from periplaneta americana inhibits oxidative stress-induced kgn cell apoptosis by regulating mitochondrial function through bcl2l13. *Reprod. Sci.* **30**(2), 473-486 (2023).
10. Wang, Q. et al. The protective effect of small peptides from periplaneta americana on hydrogen peroxide-induced apoptosis of granular cells. *In Vitro Cell. Dev. Biol.-Anim.* **57**(6), 610-619 (2021).
11. Bofill-De, R. X. et al. Structural differences between pri-mirna paralogs promote alternative drosha cleavage and expand target repertoires. *Cell Rep.* **26**(2), 447-459 (2019).
12. Christenson, L. K. Microrna control of ovarian function. *Anim. Reprod.* **7**(3), 129-133 (2010).
13. Zhang, J. et al. Downregulation of mir-192 alleviates oxidative stress-induced porcine granulosa cell injury by directly targeting acvr2a. *Cells* **11**(15) (2022).
14. He, H. et al. Mirna sequencing analysis of healthy and atretic follicles of chickens revealed that mir-30a-5p inhibits granulosa cell death via targeting

beclin1. *J. Anim. Sci. Biotechnol.* **13**(1), 55 (2022).
15. Liu, L. et al. Chi-mir-130b-3p regulates the zea-induced oxidative stress damage through the keap1/nrf2 signaling pathway by targeting sesn2 in goat gcs. *FASEB. J.* **37**(11), e23212 (2023).
16. Sun, Z. et al. Cap-mirseq: a comprehensive analysis pipeline for microrna sequencing data. *BMC Genomics* **15**(1), 423 (2014).
17. Kume, S. et al. Silent information regulator 2 (sirt1) attenuates oxidative stress-induced mesangial cell apoptosis via p53 deacetylation. *Free. Radic. Biol. Med.* **40**(12), 2175-2182 (2006).
18. Li, L. C. et al. Autophagy induced by hydrogen peroxide in porcine ovarian granulosa cells and its effect on apoptosis. Journal of Nanjing Agricultural University. **39**(05), 814-818 (2016).
19. Xiang, L., Yao, G. t., Li, R. X., Zhang, J. & Huang, Y. Z. Research progress on the establishment methods of animal models of premature ovarian failure. *Chinese Journal of Pharmacy*. **50**(05), 386-389 (2015).
20. Massin, N. et al. Evaluation of different markers of the ovarian reserve in patients presenting with premature ovarian failure. *Mol. Cell. Endocrinol.* **282**(1-2), 95-100 (2008).
21. Weng, Q. et al. Oxidative stress induces mouse follicular granulosa cells apoptosis via jnk/foxo1 pathway. *PLoS One* **11**(12), e167869 (2016).
22. Liu, Z. Q. et al. Expression of puma in follicular granulosa cells regulated by foxo1 activation during oxidative stress. *Reprod. Sci.* **22**(6), 696-705 (2015).
23. Shen, M. et al. Involvement of the up-regulated foxo1 expression in follicular granulosa cell apoptosis induced by oxidative stress. *J. Biol. Chem.* **287**(31), 25727-25740 (2012).
24. Zhang, M. et al. Mir-181a increases foxo1 acetylation and promotes granulosa cell apoptosis via sirt1 downregulation. *Cell Death Dis.* **8**(10), e3088 (2017).
25. Wang, Q. et al. The protective effect of small peptides from periplaneta americana on hydrogen peroxide-induced apoptosis of granular cells. *In Vitro Cell. Dev. Biol.-Anim.* **57**(6), 610-619 (2021).
26. Engedal, N. et al. From oxidative stress damage to pathways, networks, and autophagy via micrornas. *Oxidative Med. Cell. Longev.* **2018**, 4968321 (2018).
27. Lewinska, A. et al. Reduced levels of methyltransferase dnmt2 sensitize human fibroblasts to oxidative stress and dna damage that is accompanied by changes in proliferation-related mirna expression. *Redox Biol.* **14**, 20-34 (2018).
28. Kume, S. et al. Silent information regulator 2 (sirt1) attenuates oxidative stress-induced mesangial cell apoptosis via p53 deacetylation. *Free. Radic. Biol. Med.* **40**(12), 2175-2182 (2006).
29. Morita, Y. et al. Resveratrol promotes expression of sirt1 and star in rat ovarian granulosa cells: an implicative role of sirt1 in the ovary. *Reprod. Biol. Endocrinol.* **10**, 14 (2012).

30. Sohel, M. M. H. et al. Oxidative stress modulates the expression of apoptosis-associated micrornas in bovine granulosa cells in vitro. *Cell. Tissue. Res.* **376**(2), 295-308 (2019).
31. Liu, S.Y. Mechanism study of Periplaneta Americana regulating mir-29a/pten/pi3k to intervene in Ulcerative Colitis in mice. *Guangzhou University of Chinese Medicine*, 2023.
32. Penna, E., Orso, F. & Taverna, D. Mir-214 as a key hub that controls cancer networks: small player, multiple functions. *J. Invest. Dermatol.* **135**(4), 960-969 (2015).
33. Yang, S. et al. Mirna-214 suppresses oxidative stress in diabetic nephropathy via the ros/akt/mtor signaling pathway and uncoupling protein 2. *Exp. Ther. Med.* **17**(5), 3530-3538 (2019).
34. Chen, W. et al. Microrna-214 protects l6 skeletal myoblasts against hydrogen peroxide-induced apoptosis. *Free Radic. Res.* **54**(2-3), 162-172 (2020).
35. Wang, F., Liu, M., Li, X. & Tang, H. Mir-214 reduces cell survival and enhances cisplatin-induced cytotoxicity via down-regulation of bcl2l2 in cervical cancer cells. *FEBS Lett.* **587**(5), 488-495 (2013).
36. Yang, L., Zhang, L., Lu, L. & Wang, Y. Mir-214-3p regulates multi-drug resistance and apoptosis in retinoblastoma cells by targeting abcb1 and xiap. *OncoTargets Ther.* **13**, 803-811 (2020).
37. Zhang, J., Su, B., Gong, C., Xi, Q. & Chao, T. Mir-214 promotes apoptosis and sensitizes breast cancer cells to doxorubicin by targeting the rfwd2-p53 cascade. *Biochem. Biophys. Res. Commun.* **478**(1), 337-342 (2016).
38. Huang, Q. et al. Effects of miR-103a-3p on proliferation and apoptosis of ovarian granulosa cells. *Journal of Xiangnan University (Medical Edition)*. **24**(04), 1-6 (2022).
39. Zhou, Y. P. & Xia, Q. Inhibition of mir-103a-3p suppresses lipopolysaccharide-induced sepsis and liver injury by regulating fbxw7 expression. *Cell Biol. Int.* **44**(9), 1798-1810 (2020).
40. Zhang, Q. et al. Roles of mir-10a-5p and mir-103a-3p, regulators of bdnf expression in follicular fluid, in the outcomes of ivf-et. *Front. Endocrinol.* **12**, 637384 (2021).
41. Cheng, M. & Wang, Y. Downregulation of hmgb1 by mir-103a-3p promotes cell proliferation, alleviates apoptosis and in flammation in a cell model of osteoarthritis. *Iran. J. Biotechnol.* **18**(1), e2255 (2020).
42. Benco, A. et al. Involvement of the transcription factor stat1 in the regulation of porcine ovarian granulosa cell functions treated and not treated with ghrelin. *Reproduction* **138**(3), 553-560 (2009).
43. Jafarzadeh, A. et al. Microrna-383: a tumor suppressor mirna in human cancer. *Front. Cell. Dev. Biol.* **10**, 955486 (2022).
44. Gu, B., Wang, J., Song, Y., Wang, Q. & Wu, Q. Microrna-383 regulates cell viability and apoptosis by mediating wnt/beta-catenin signaling pathway in non-small cell lung cancer. *J. Cell. Biochem.* **120**(5), 7918-7926 (2019).
45. Li, Z. M. Li, W. Mir-383 suppresses proliferation of mouse follicular granulosa

cells by downregulating cyclin-related proteins. *Journal of Cellular and Molecular Immunology*. **35**(06), 518-525 (2019).

46. Liu, Y., Wang, Z., Tang, Z., Fu, Y. & Wang, L. Mirna-383-5p functions as an anti-oncogene in glioma through the akt/mtor signaling pathway by targeting vegfa. *Curr. Cancer Drug Targets* **24**(4), 463-475 (2024).
47. Li, Y. Research on the mechanism of mir-383-5p regulating apoptosis in ovarian granulosa cells. *Hebei Medical University*, 2022.
48. Zhang, H. B. et al. Identified variably spliced genes in resveratrol-induced apoptosis of porcine ovarian granulosa cells through RNA-seq screening. *China Animal Husbandry Magazine*. **58**(08), 36-44 (2022).
49. Zhang, C. et al. Mirnas expression profiling of rat ovaries displaying pcos with insulin resistance. *Arch. Gynecol. Obstet.* **302**(5), 1205-1213 (2020).
50. Lin, J. et al. Cytochrome p450 family proteins as potential biomarkers for ovarian granulosa cell damage in mice with premature ovarian failure. *Int. J. Clin. Exp. Pathol.* **11**(8), 4236-4246 (2018).
51. Tosca, L., Chabrolle, C. & Dupont, J. [Ampk: a link between metabolism and reproduction?]. *M S-Med. Sci.* **24**(3), 297-300 (2008).
52. Brunk, U. T., Neuzil, J. & Eaton, J. W. Lysosomal involvement in apoptosis. *Redox Rep.* **6**(2), 91-97 (2001).
53. Guicciardi, M. E., Leist, M. & Gores, G. J. Lysosomes in cell death. *Oncogene* **23**(16), 2881-2890 (2004).